Combined use of geophysical methods and remote techniques for characterizing the fracture network of a potential unstable cliff site (the "Roche du Midi", Vercors massif, France)

Jacques Deparis, Bruno Fricout, Denis Jongmans, Thierry Villemin, Laurent Effendiantz, Alex Mathy

Combined use of geophysical methods and remote techniques for characterizing the fracture network of a potential unstable cliff site (the "Roche du Midi", Vercors massif, France)

J. Deparis[1], B. Fricout[2], D. Jongmans[1], T. Villemin[2], L.Effendiantz[3], A.Mathy[4]

[1]LGIT, Université Joseph Fourier Grenoble, BP53, 38041 Grenoble Cedex 9, France
[2]LGCA, UMR 5025, Université de Savoie, 73376 Le Bourget du Lac Cedex, France
[3]CETE Lyon, 25, avenue François Mitterrand, 69674 BRON CEDEX, France
[4]SAGE, 2 rue de la Condamine F - 38610 Gières, France

E-mail : denis.jongmans@ujf-grenoble.fr

Abstract Stability assessment of a cliff strongly depends on the fracture pattern and the face topography. Geological observations as well as classical geodetic measurements are difficult to perform on high nearly vertical cliffs like the ones surrounding the town of Grenoble (French Alps). In this study we combine remote and ground imaging techniques for characterizing the geometry and the fracture pattern of potential unstable cliff sites. A Dense Digital Surface Model (DDSM) of the rock face can now be obtained from laser scanning (Lidar) or photogrammetry. These techniques are safer and quicker than direct measurements. They offer the possibility to collect structural data and to sample the shape of the outcrop at a centimetric resolution. We applied these two techniques to a potential unstable site (the "Roche du Midi", Vercors massif) for determining the main fracture families affecting the rock mass and we obtained results similar to direct measurements performed on the nearby outcrops and on the cliff face itself. The laser scanning data suffers a bias in the illumination of the site. Geophysical experiments were also conducted on the plateau and on the cliff face in order to delineate the fracture pattern inside the rock mass. ERT (Electrical Resistivity Tomography) and GPR (Ground Penetrating Radar) profiles were performed on the plateau and allowed near-vertical open fractures to be located in the vicinity of the surface. Best geophysical results in terms of penetration and resolution were however obtained from GPR profiles conducted directly on the cliff face. Laser scanning data were combined with GPR data in order to take into account the shape of the sampled profiles. The combination of vertical and short horizontal profiles allowed the strike and dip of the discontinuities to be determined. The two main families were imaged, as well as a major continuous inward dipping reflector which was not shown during the initial reconnaissance. Further investigation inside the mass effectively showed the existence of this fracture. These results highlight the power of the GPR technique in characterizing the discontinuity pattern inside rock mass for improving the model in view of hazard assessment.

Keywords : Stability assessment, fracture, Digital Surface Model, laser scanning, GPR, Rockfall.

Submitted to: Journal of Geophysics and Engineering

1. Introduction

Rock falls pose critical problems to risk management in mountain areas, due to the suddenness of the phenomena and the lack of evident precursors. In addition, hazard assessment in such context is made problematic by, first, the difficulty to perform surface observations, second the lack of information about the internal structure of the rock mass and, third, the little knowledge about the triggering mechanism (Hantz et al, 2003). Estimation of the rock mass stability requires detailed investigations of the discontinuity pattern (Hoek and Bray, 1981). However, measurements performed on top of the cliff or on the face itself does not provide all the needed inner information. Moreover, data collection on the cliff requiring abseiling is time consuming and can be highly-risky. For these reasons, we tried to improve the quality and efficiency of site investigation and geological data collection in cliff context and for volumes ranging from a few thousands m^3 to a few hundred of thousands m^3. The proposed methodology combines three types of investigations: a structural analysis based on surface observations and remote measurements, the collection of a dense digital surface model (DDSM) of the

cliff obtained from laser scanning, and geophysical experiments including GPR (Ground Penetrating Radar) measurements.

Resorting to remote techniques (Peterson et al., 1982) is obvious where multiple difficulties stand in the way to direct measurements, which is the case at the surface of cliffs. The most common one is photogrammetry which requires a stereoscopic pair of photographs (Mikhai et al., 2001). As the surface to be studied is nearly vertical, the photographs should be horizontal or oblique views of the site. Large scales ranging from 1/500 to 1/2000 are usual. Provided the inner and outdoor orientation is known accurately for each photo, the 3D coordinates of each pixel can be computed insofar as homologous pixels are identified on both images of the stereoscopic pair. Manual or computer-aided techniques exist for pointing homologous pixels. As far as series of points are localised, the position and orientation of geological structures can be evaluated. This method enables us to complete the structural analysis of the cliff site. Airborne laser scanning techniques are now commonly used for varied applications in Earth Sciences. This includes, among others, geomorphologic mapping in mountain areas (van Asselen and Seijmonsbergen, 2006), river bank erosion and topographical changes (Thoma et al, 2005; Chen et al, 2006), and landslide detection and mapping (McKean and Roeging, 2004; Glenn et al, 2006; Ardizzone et al., 2007; Schulz, 2007). The use of terrestrial laser scanners is also continuously increasing, with a wide range of applications in architecture and civil engineering (Schulz and Ingensand, 2004; Tsakiri et al., 2006). These techniques were also used in rock engineering, since they provide a detailed representation of rock surfaces (Schulz et al., 2005). Recent studies have focused on the characterization of geological discontinuities from laser point clouds (Feng and Röshoff, 2004; Lemy and Hadjigeorgiou, 2004). They showed that a good agreement can be reached between on-site measurements and laser scan measurements, provided that the density of points is high enough. Bornaz and Dequal (2003) proposed the concept of the Solid Image combining laser scanning data and a co-registered image. Because important structural features may be ignored or misread when texturing a DDSM (Dense Digital Surface Model) with radiometric data, the solid image approach keeps the image in its original geometry and resolution, and re-projects DDSM data (like point clouds obtained from laser scanning systems) on the image itself. If the point clouds are dense enough, this allows localizing each pixel. Measurements like fractures orientation on a rock surface can then be easily made by selecting areas and computing the best fitting surface. In addition, following the trace of fractures or bedding planes on the images directly gives a 3D digitizing of the trace. Compared to a photogrametric approach, a solid image interpretation is simpler to implement, quicker to use and does not require special training.

A major issue for assessing the rock fall hazard is the persistence of fractures inside the rock mass. Since geological observations and rock surface analysis can not provide this information, geophysical techniques were applied on the study site. Geophysical methods are increasingly used for cliff (or high slope) investigations, both on the top (Dussauge et al., 2003; Busby and Jackson, 2006, Heincke et al., 2006) and on the cliff face (Dussauge et al., 2003; Roch et al., 2006; Jeannin et al., 2006; Deparis et al., 2007). Geophysical investigation on the plateau may provide valuable information about the continuity of outcropping structures (fractures, faults) or the rock quality. Heincke et al. (2006) applied the 3D tomographic seismic refraction technique over the scarp of the Randa rockfall (Switzerland). The 3D tomogram revealed the presence of a huge volume of very low P-wave velocity rock extending to more than 35 m depth. Even in this case, the investigation depth is however low compared to the scarp height (a few hundreds of m) and the method resolution decreases with depth. When possible, the use of GPR on the cliff face was found to be the most valuable tool in terms of resolution for investigating a rock mass (Jongmans and Garambois, 2007). The main two limitations of GPR for cliff investigation are safety requirements for abseiling and the penetration depth which can be diminished by the high electrical conductivity. In the Mesozoic limestone rocks outcropping around the town of Grenoble (French Alps), the maximum penetration is about 30 m with 100 MHz antennae (Dussauge et al., 2003 ; Jeannin et al., 2006).
This paper presents the investigation results for a cliff site (the “Roche du Midi”) located in the French sub-alpine limestone Massif of Vercors. The study aims at testing the capacities of laser scanning (using the concept of solid image) and geophysical prospecting methods for characterizing the fracturing on a potential unstable site and at showing the effectiveness of combining the two

techniques in cliff site investigations. Compared to previous studies where GPR was used in similar conditions (Dussauge et al., 2003; Roch et al., 2006; Jeannin et al., 2006; Deparis et al., 2007), the cliff height (200 m) is one order of magnitude greater, which posed additional operational difficulties.

2. Description of the site

The "Roche du Midi" site is located in the Vercors Massif, 30 km north-west of Grenoble (figure 1). The Vercors massif belongs to the external thrust belts of the western alpine chain (Philippe et al., 1998). Morphologically it corresponds to a group of plateaux reaching an elevation between 1,000 m and 2,000 m and limited by near vertical cliffs. These are mainly made of massive limestone, dated back to Lower Cretaceous (Urgonian limestone, figure 1). The height of the cliffs range from 50 m to 400 m. Initial bedding has been folded and faulted during the alpine tertiary shortening. It results mostly in subvertical strike-slip faults associated to large thrust zones (Arnaud et al., 1978; Philippe et al., 1998).

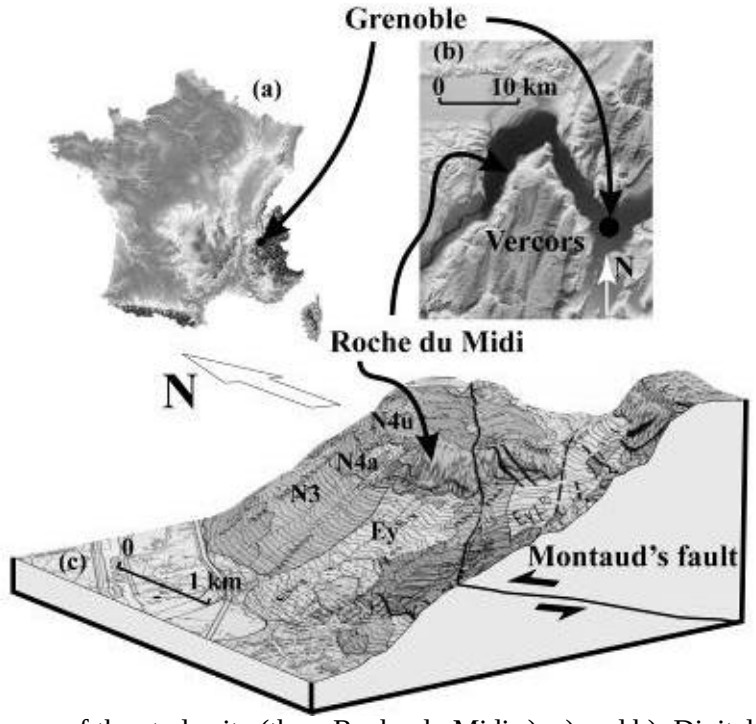

Figure 1: Location map of the study site (the « Roche du Midi »). a) and b): Digital elevation model of France and of the Vercors Massif, respectively. c) Geological map (from Gidon et al., 1978) draped on the digital elevation model. N3 and N4a : moderate slope in marls; N4u: vertical cliff in the Urgonian limestones; Ey: superficial scree deposits. The reverse Montaud's fault is indicated.

The "Roche du Midi" site is a 200 m high cliff striking N-S (figures 1c and 2). The rock is a fine grained limestone of lower Urgonian in age with lateral facies changes. The bedding is nearly horizontal. The top of the cliff is made of a plateau at an elevation of about 1240 m and covered by pine trees. A one meter opening fracture (F_1) striking N140°E is visible north of the site where it intersects the cliff (figure 2). This fissure penetrates the rock mass and its trace is lost about 30 m SW of its issue on the cliff (figure 3).

A structural study was first performed on the nearby outcrops both on the plateau (figure 4a) and on the vertical cliff (figure 4b) with alpine technique. Thirty-five fracture planes were measured (dip-direction and dip) on the plateau outcrops, at a maximum distance of 500 m from the site, with a clinometer-compass giving an angular accuracy of about 5° (data set DM1). Due to technical difficulties when abseiling, only 22 strike values of fracture plane were measured on the cliff face itself (data set DM2). Two main near-vertical fractures families (labelled F_a and F_b,), striking N10°E-N40°E and N120°E-N150°E on average are present on the site. Even though no slickensides have

been observed on the fractures themselves, F_a and F_b could be originally conjugate shear fractures, oriented in accordance with strike-slip faults mapped in the area and striking in the same directions (Arnaud et al., 1978; Arpin, 1988).

We have drawn a sketch map of the plateau (figure 3). Presence of fresh lapies shows active karstic erosion on this site. Fractures F_a are more or less parallel to the scarp face, whereas F_b fractures intersect it obliquely. The main open fracture F_1 is globally oriented N130°, based on a system of F_b and F_a families in relay (figure 3). The opening of F_1 ranges between 40 cm to 1 m and the fracture was recognized on a depth of 60 meters above the ground.

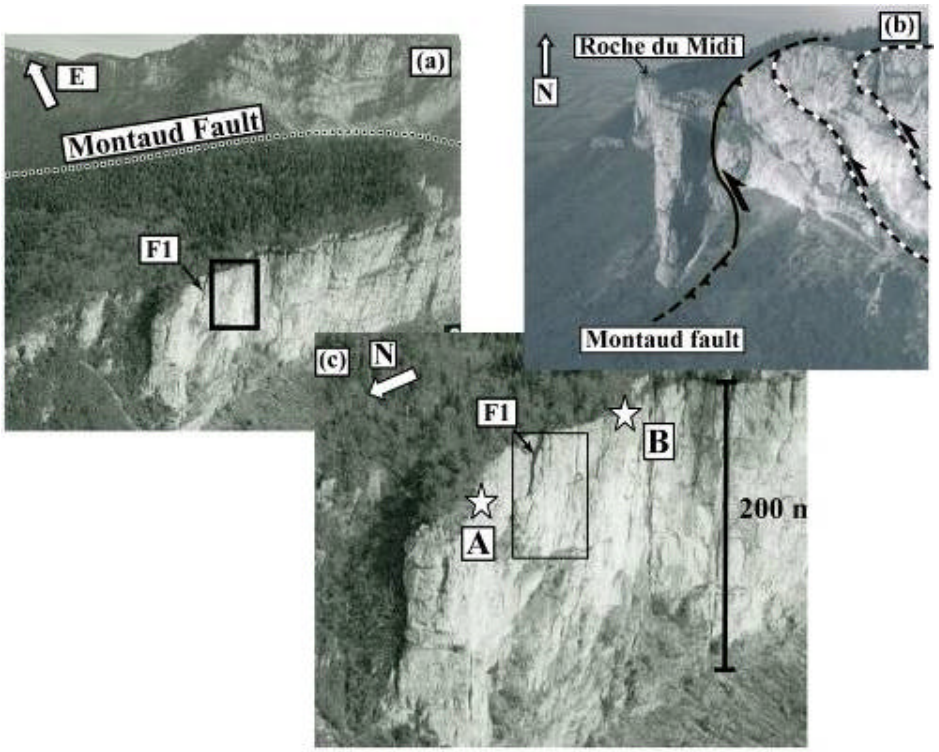

Figure 2: a) and b) Aerial photos of the site taken from the NW and the S, respectively, with the location of the Montaud fault and some secondary faults. c) Zoom of picture a) with the Lidar sources points A and B (white stars, see text for the explanation of the geometry acquisition). The rectangle shows the study site.

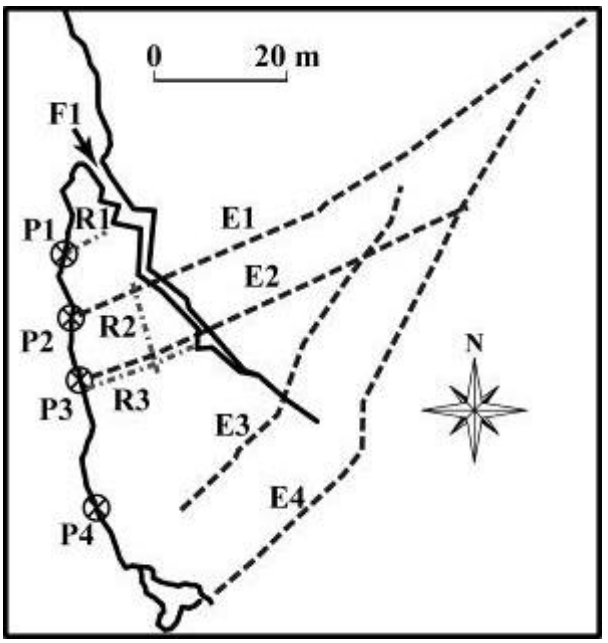

Figure 3: Schematic map of the plateau with the location of the major outcropping fracture F_1 and of the geophysical profiles. P1 to P4: vertical GPR images. R1 to R3: horizontal GPR images on the plateau. E1 to E4: electrical profiles on the plateau.

3. Laser scan and photogrammetry measurements

3.1. Acquisition

Laser scanner acquisitions were made from two different locations A and B with a distance of about 100m to the cliff centre (figure 2). Two acquisitions were necessary in order to increase the sampling of the cliff and to avoid or to restrict darkness areas. The Instrument used was a Riegl Z420i. This instrument has a scanning range of 0° to 360° and 0° to 80° for the horizontal and vertical frame, respectively. The first location point A, north of the cliff, looked at the outcrop in a N140°E ±10° direction with a dip ranging from +5° to -50° relative to the horizontal plane. The second one (B), south of the cliff, looked at the outcrop in a N30°W±20° direction with a dip of 0° to -60°. These two acquisition points allowed ten and five millions points to be acquired, respectively, with almost no overlap. The angular step of the scan being about 2.10^{-2} degree gives a spatial resolution of four centimeters before filtering.

Laser data were filtered using median filter in order to eliminate outliers and to reduce noise in the data set. After filtering, the mean spatial resolution is only 10 cm, (for a theoretical accuracy of one cm). Each point cloud was triangulated in spherical geometry, using only laser coordinates (azimuth and dip, Alberts, 2004). This way of processing gives a two-dimensional triangulation which leads to a DDSM close to the real surface. Retroreflective artificial targets (~10 cm^2) were stuck on the cliff, measured and used to calculate the position and the orientation of each scan in a reference frame, north and horizontally oriented.. Common artificial targets allow the two point clouds to be coregistered into a single 3D model. The result of the terrestrial laser scanning is presented on figure 5. The DDSM covers about 75% of the cliff surface and exhibits shadow regions resulting from the low incidence angles of the laser with respect to the cliff face.

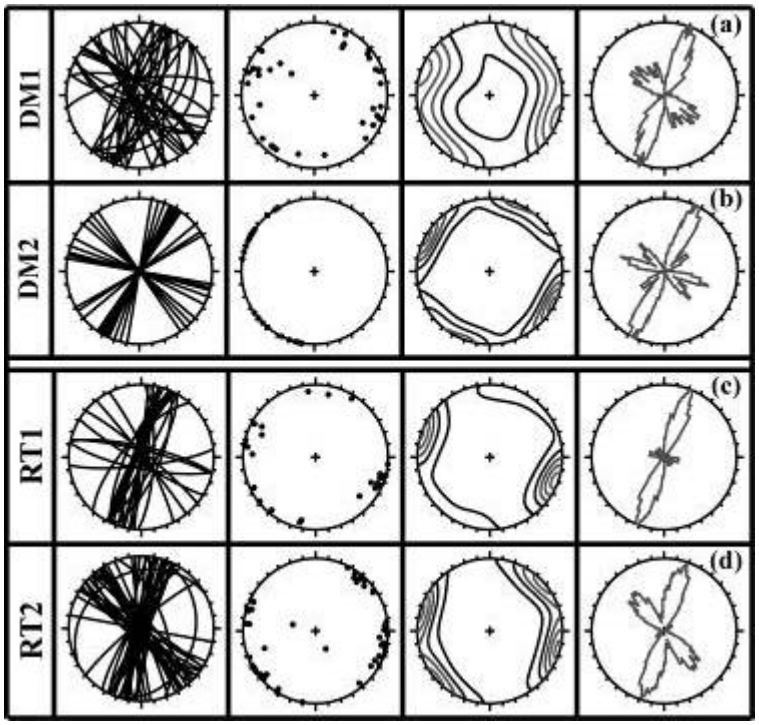

Figure 4. Stereograms (Schmidt's lower hemisphere projection) and rose diagrams for the four collected structural data sets. DM : Direct Measurements; RT: measurements remotely performed (a) DM1: plateau outcrops (b) DM2: cliff outcrops, (c) RT1: solid image and (d) RT2: photogrammetry. First column: great circles of fracture planes, second column: poles to fractures planes, third column: pole contour diagram. Fourth column: Moving average rose diagram performed on strike with a 10° aperture. 35, 22, 28 and 47 values were displayed for DM1, DM2, RT1 and RT2 techniques, respectively.

A series of eight stereoscopic photographs with parallel and horizontal axes and an overlap of 80% on average were taken from a helicopter at a distance of about 100 m from the cliff. The camera used was an UMK 1318 with a 100 mm focal length, providing silver images, 18-13 cm in size and 1/1000 in scale. All films were digitized in images of ~14,000*10,000 pixels. One pixel corresponds to a surface on the cliff of about 4 by 4 cm. Cross marks were painted on the cliff before flying. The location of these marks was measured in the field and allowed us to use ground control points for computing the outdoor orientation of all photos and of each stereoscopic pair.

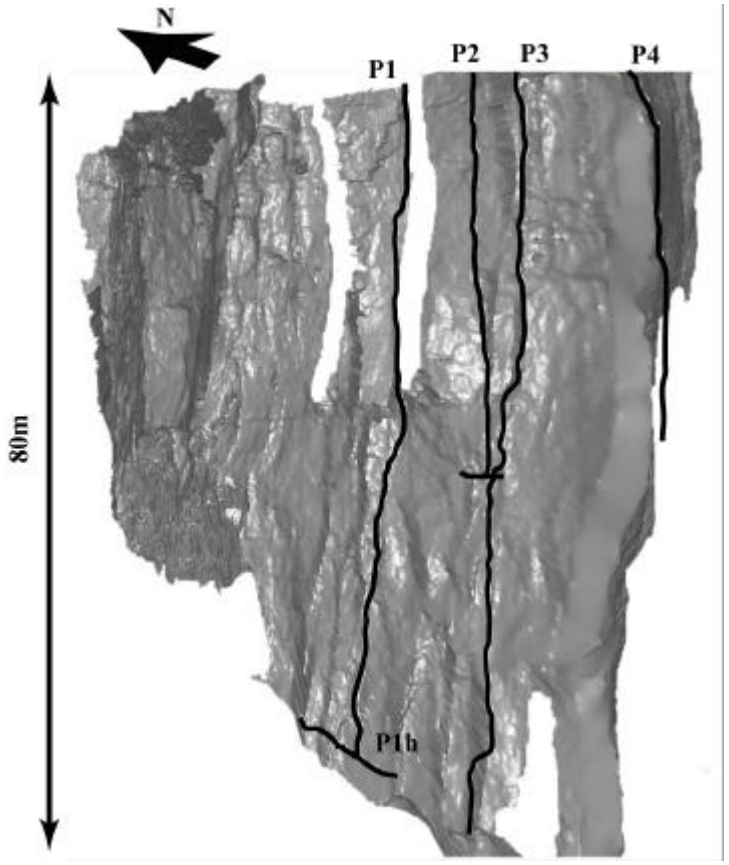

Figure 5: DDSM (Dense Digital Surface Model) of the site obtained from the processing of the two sets of laser scanning data, with the location of the GPR scan data collection lines P1, P2, P3 and P4 (in black).

3.2. Structural Analysis

No structural analysis was directly made on the DDSM of figure 5. For such analysis, we used a solid image approach (Bornaz and Dequal, 2003), which consists in using single original images, in their initial geometry, combined with 3D-location information for each pixel. Since no resampling of the image was needed we avoided the huge distortion that appears locally in such processing. We have then selected specific zones on the image that could correspond to fractures. The planar or non planar properties of these zones were tested using a least square adjustment. We only kept 40 zones that were enough planar and could be fractures. Structural results of this analysis (data set RT1) are showed in figure 4c. In addition to this approach, we also performed photogrametric measurements. As the central couple of photos displays most entirely the studied area, we only used a single couple for structural analysis purposes. 50 fractures at different places on the cliff were measured. As for the solid image approach, a planar adjustment has been made on a few points measured on each surface. Figure 4d displays the data collected (RT2). The two families F_a and F_b are represented. Bedding attitude was also measured at two different places. There is no evidence on the cliff of fractures with an orientation different from those measured in the plateau.

4. Geophysical measurements

Two geophysical campaigns were performed on the site, one on the plateau and one on the cliff face.

4.1. Experiments on the plateau

The geophysical experiments on the plateau included four electrical tomography profiles and three GPR lines, the location of which is given in figure 3. The electrical profiles (labelled E1 to E4) were carried out perpendicularly to the cliff face in order to pinpoint the open fractures crossing the surface and to characterize the rock mass resistivity values. The Wenner alpha array configuration was chosen for its robustness (Dahlin and Zhou, 2004). The electrode spacing was 2 m for profiles E1, E3 and E4 and 1 m for profile E2. Inversion of apparent resistivity values was made using the software RES2DINV with the L1 norm (Loke and Barker, 1996, Loke, 2000) . Electrical images obtained after 5 to 6 iterations and with a RMS lower than 3% are shown in figure 6. The influence of the 200 m high cliff on apparent resistivity measurements was not corrected, as this effect would regularly increase the apparent resistivity values by a factor between two near the cliff edge and one at the farthest distance (Sahbi et al., 1997). Thus, strong lateral contrasts which are the targets of this study and 10 meters away from the cliff (figure 6) are little affected by the presence of it. Electrical resistivity in the rock exhibits a large range of values from 50 O.m in the highly weathered clayey zones, to more than 5000 O.m in the open fracture. The mean resistivity of the rock mass varies between a few hundreds O.m and 1500 O.m on the four profiles. Considering the reduction factor due to the cliff influence, these relatively low values characterize a weathered or slightly marly limestone (Reynolds, 1997). A strong vertical resistive anomaly appears on profiles E1 and E2 at a distance of 14 and 18 m from the cliff edge, respectively. This anomaly corresponds to the open fracture F_1 observed on the plateau. Further south, this structure is still displayed on the E3 tomography by a narrow and shallow resistive anomaly, which indicates that the fracture closes laterally and at depth. This interpretation is also supported by profile E4 where the fracture is not visible anymore. Beyond a distance of 60 m from the cliff, the long profiles E1 and E4 show a strong resistivity decrease eastward, from 1400 Ωm to 250 Ωm. As the bedding is near-horizontal, this lateral resistivity decrease within the limestone results from a highly fractured and weathered zone. Along all the electrical images, superficial high resistive spots are observed, which could correspond to open fractures of lesser importance than F_1 are. The three GPR images (figure 6b) performed with 100 MHz unshielded antennae are presented with a depth vertical axis, considering a velocity of 10 cm/ns deduced from a CMP velocity analysis. GPR data show one or two main near-horizontal reflectors down to 5 to 8 m deep, corresponding to major bedding planes. Irregularities along the reflectors could reflect the presence of karstic phenomena. On profile R3, a 1.5 m wide vertical air-filled fracture is evidenced by the ringing response in the data between 4.8 and 6.3 m.

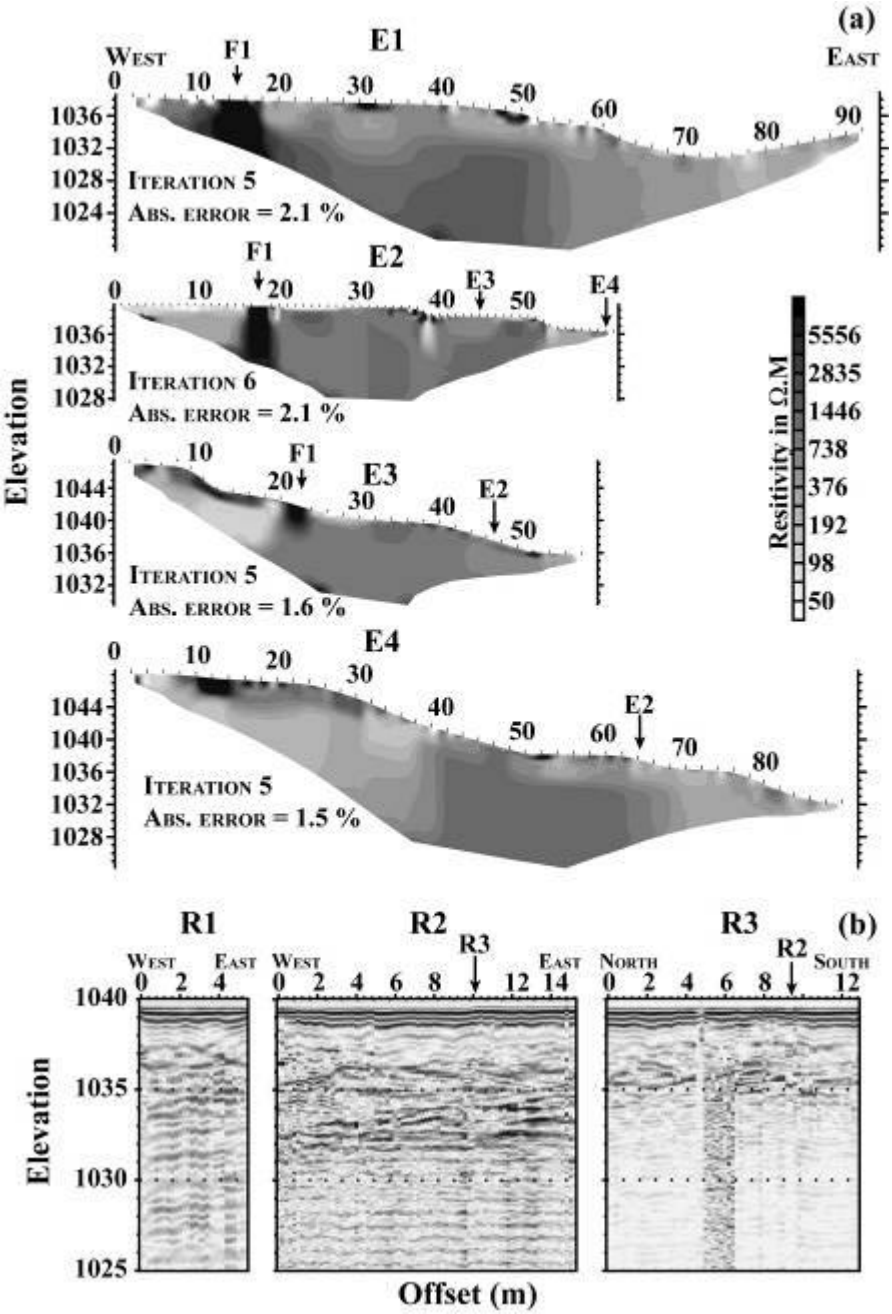

Figure 6: Geophysical experiments on the plateau. (a): Electrical tomography profiles E1 to E4. (b): GPR images R1 to R3 measured with a 200 MHz antennae.

Both surface electrical and GPR experiments show the presence of near-vertical fractures within the limestone with, however, little information on the geometry and continuity of these discontinuities at depth. GPR on the plateau is not designed for imaging near-vertical reflectors and the penetration depth of the radar waves is severely limited by the shallow conductive zones (< 200 O.m) pointed out on electrical images. Electrical tomography allows the location of superficial resistive open fractures but the penetration is limited by the profile length and the resolution of the electrical image dramatically decreases with depth, making the method poorly adapted for deep investigation purposes.

4.2. Experiments on the cliff face

To overcome these limitations and as the rock mass offers the required safety conditions for abseiling, four vertical GPR scans (P1 to P4) and two short horizontal ones (P1h and P2h) were directly performed on the cliff face (see Figs. 3 and 5). The lengths of profiles P1, P2, P3 and P4 are 65 m, 45 m, 31 m and 52 m, respectively. Measurements were made with a RAMAC system and 100 MHz unshielded antennae (TE mode) which offer a good compromise between resolution and penetration in this type of limestone (Jeannin et al., 2006). The trace spacing was 20 cm. The cliff height made impossible any operation from the bottom and required the presence of two experimented climbers on independent ropes for safety requirements. Reflecting artificial targets were placed along the profiles on the cliff face for positioning the measurements during the laser scanning. The targets, having a higher reflectivity, can easily be differentiated and their coordinates were extracted for locating the GPR experiments. In order to compute the complete 3D traces of the GPR profiles we interpolated intermediate points by computing the intersection between the triangulated DDSM and the vertical plane going through two consecutive targets. The 3D trace was then given with one point each 10 cm. GPR traces are superimposed on the DDSM (figure 5).

The six profiles acquired with 100 MHz antennae are presented in figure 7, considering a mean velocity of 10 cm/ns and the topography given by the DDSM. Since reflectors are almost horizontal and no diffracted wave is visible, no migration process was applied to the data, preventing the appearance of undesirable noise. Figure 7 clearly shows contrasted results in terms of reflectivity and penetration. The maximum penetration (about 25 m) was obtained at the bottom of profile P1 and along profile P4, while profile P3 shows much less penetration (10 m) with a high attenuation of radar waves, probably resulting from the highly fractured and weathered zone observed on the cliff. To 15 m depth, profiles P1, P2 and P4 display several near-vertical continuous reflectors (labelled F_a and F_b in Figs. 7e and 7f) showing local dip variations when they intersect inclined fractures. Examination of the horizontal profiles P1h and P2h performed at the bottom of profiles P1 and P2 shows that these near-vertical discontinuities have mainly two orientations (N20°E and N130°E) which agree with the two fracture families F_a and F_b pointed out by the geological study. No such information is available for profile P4. The open fracture F_1 observed on the plateau with an aperture of 50 cm to 1m does not appear as a major reflector on the vertical profiles P1, P2 and P3, but rather as several weak and discontinuous reflectors (figures 7a, 7b and 7c). Our interpretation is that this reflectivity pattern results from the non planar geometry of F_1, which is made as a succession of short fractures of the two families F_a and F_b (see figure 3), generating several reflections and scattering from different azimuths with similar travel times. On profile P3, the strong wave attenuation makes the fracture hardly visible. On the contrary, F_1 appears as a continuous reflector at 21 m depth on profile P4 (figure 7d), where F_1 has a linear trace at the surface (figure 3). Below the elevation of 1215 m, the reflection separates in two branches, probably due to an increase of the aperture of the fracture, which becomes greater than $\lambda/2$ (Widess, 1973). Assuming an Air filling and a central frequency of 100 MHz for the antennae, the fracture should be over 1.5 m wide. Surprisingly, the strongest and more continuous reflector appearing on profile P1 (labelled F_2) is an inward E dipping discontinuity fracture and oriented parallel to the cliff face (N10°E - 45°E to 70 °E). This discontinuity, which is visible on the four profiles, deepens eastward and does not reach the surface, being systematically cut by a near-vertical fracture. It was not detected during the first phase of the geological investigation and its interpretation will be discussed in section 5.

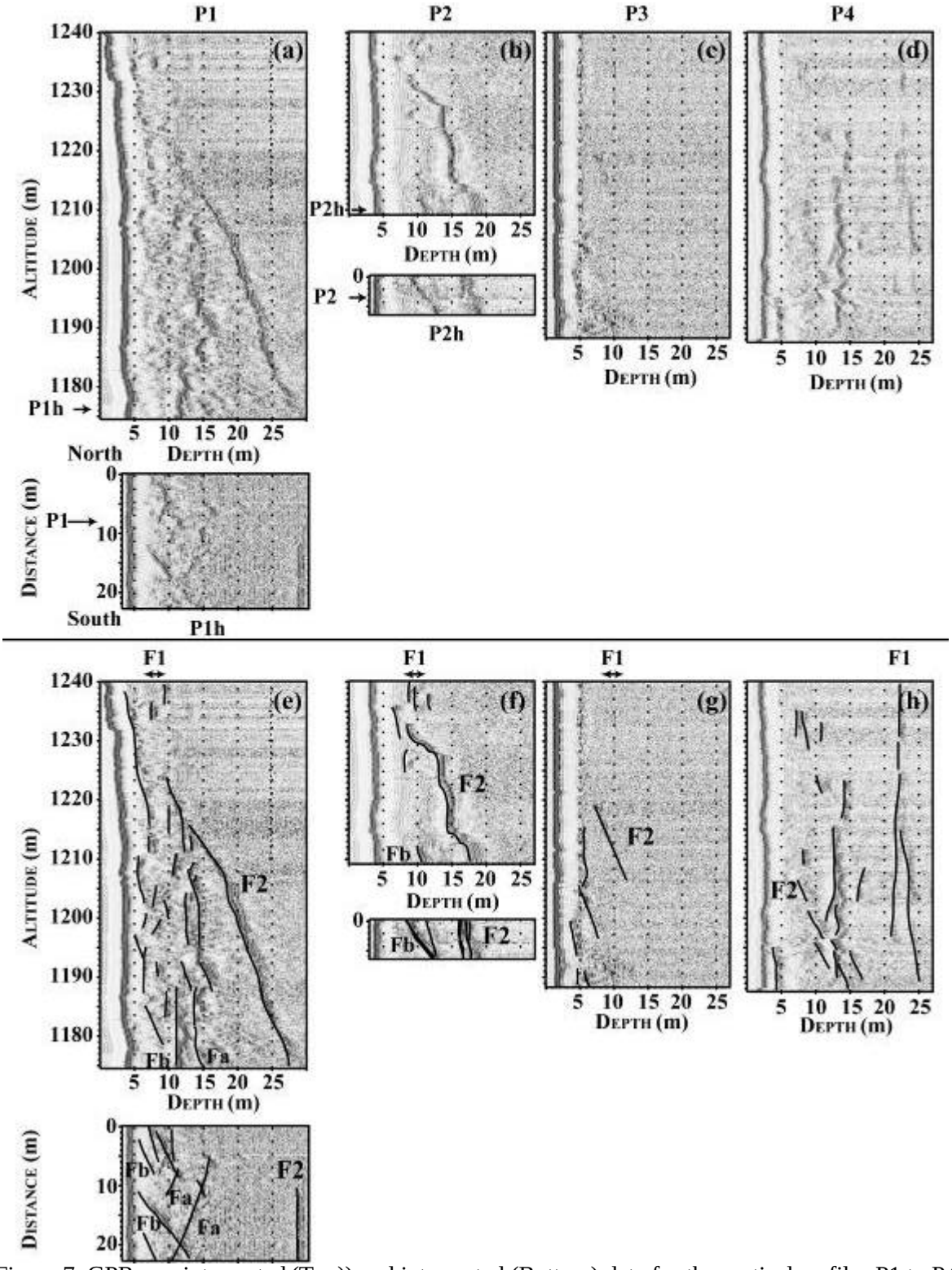

Figure 7: GPR non interpreted (Top)) and interpreted (Bottom) data for the vertical profiles P1 to P4 and the horizontal profiles P1h and P2h. acquired with 100 MHz antennae. Thin black line correspond to fracture detected by GPR.

Figure 8 displays the GPR images acquired with the 200 MHz antennae in the TE and TM modes along profile P1. Comparison of these two diagrams with the 100 MHz image (figure 7a) points out an improvement of the resolution for a similar penetration depth when using the 200 MHz antennae. At an elevation between 1200 m and 1225 m, two near-vertical reflectors can be distinguished at about 2 m and 5 m deep (figures 8a and b), whereas one single reflector is visible using the 100 MHz antennae

(figure 7a). Also, the geometry of reflector F_2 is more accurately imaged in figure 8 which clearly shows that this fracture dipping to the east ends on a near vertical fracture located at 3 m from the cliff face. The GPR images obtained with two different modes (figure 8) are consistent, but exhibit differences resulting from the variations of reflection coefficients on the interfaces. Even if this information could be valuable for assessing the properties of the fracture (aperture and filling, Deparis et Garambois, 2006), it is probably not worth performing the two acquisitions in such difficult conditions.

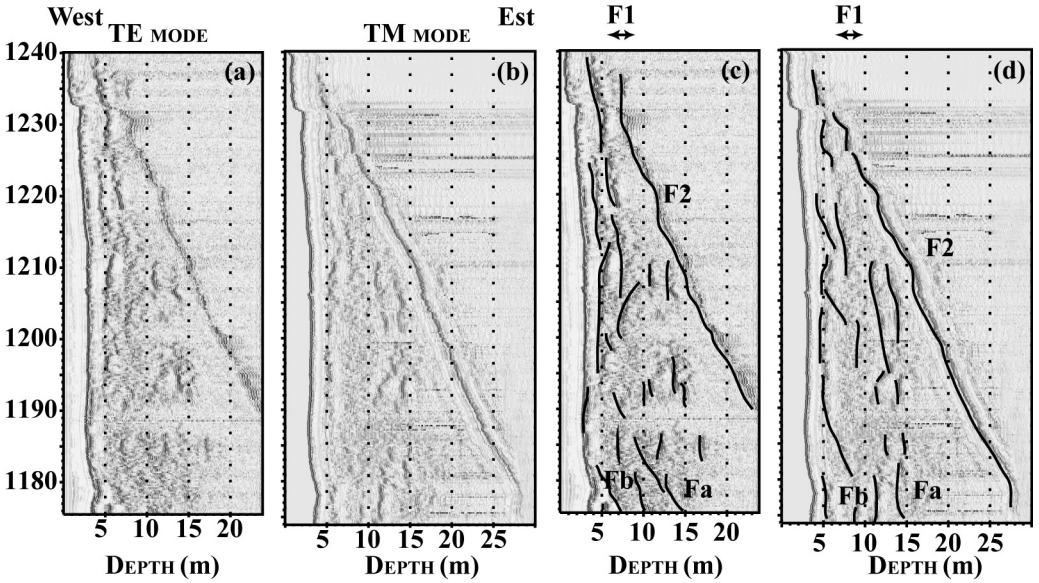

Figure 8: GPR non interpreted (a, b) and interpreted (c, d) data for the vertical profile P1 acquired with a 200 MHz antennae for the TE (a, c) and TM modes (b, d),

5. Investigation of fracture F_1

The major reflector F_2 was not detected during the initial geological investigation. A further exploration of the karstic network affecting the rock mass was decided from the open fracture F_1. Figure 9a shows a picture taken at about 10 m depth inside this fracture, with a vertical downward view. This picture clearly points out that the F_1 fracture is made of a relay of F_a and F_b discontinuities with a predominance of F_b fractures (figure 9b). Below 20 m, F_1 was found to be cut by an inward SE dipping fracture striking N30°. The vertical sketch made from the observations (figure 9c) shows that the fracture dip is 45° at a depth of 20 m and increases to 70° between 25 m and 40 m deep. These results are remarkably consistent with the geometry of the reflector F_2 shown on the close P2 profile (compare figures 9c and d). This major discontinuity, whose existence was impossible to detect from the surface, is parallel to the Montaud's fault located 250 m from the site (figure 2) and is probably a branch of this thrust fault. These results highlight the interest and the power of GPR methods for characterizing the discontinuity pattern inside the rock mass.

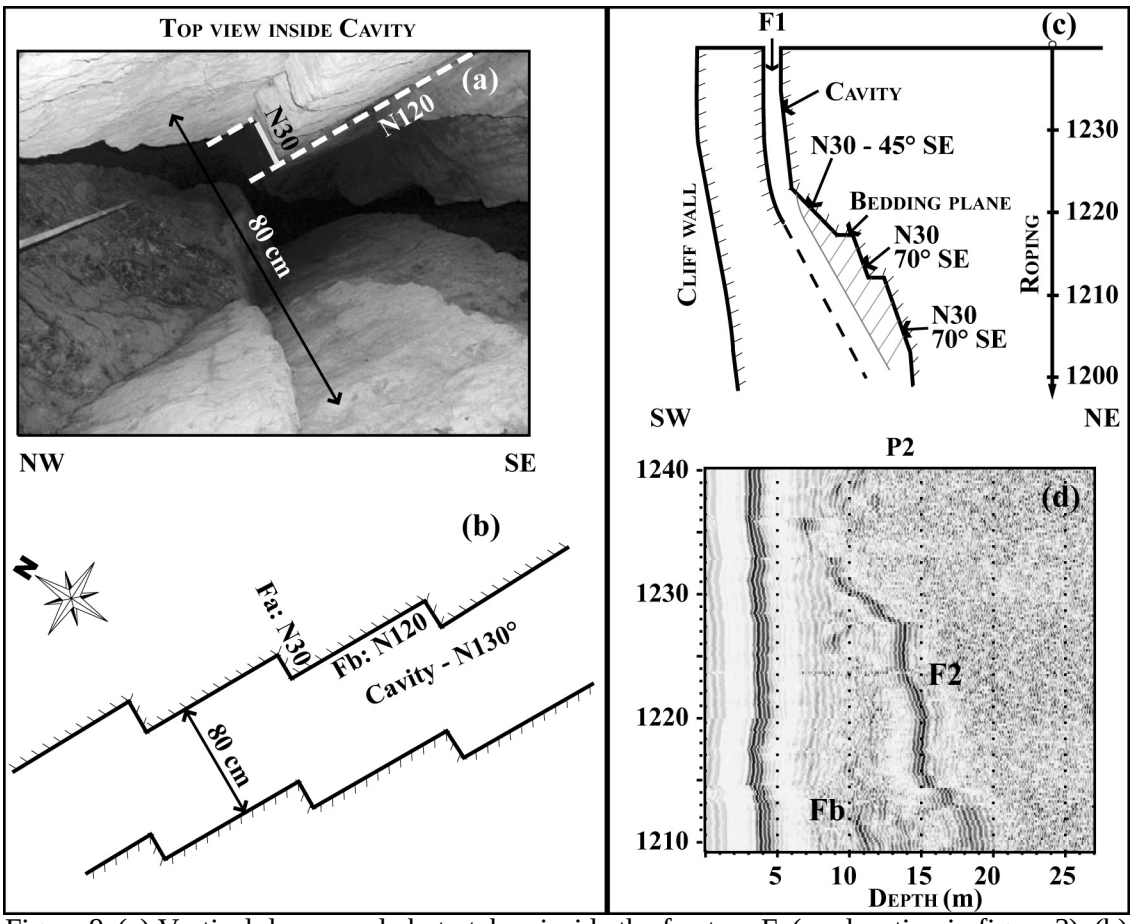

Figure 9: (a) Vertical downward photo taken inside the fracture F_1 (see location in figure 3). (b) Horizontal schematic cross-section through F. (c) Vertical sketch of the F_1 fractre. (d) GPR data for the vertical profile P2.

6. Discussion and conclusion

Measuring the fracture pattern within a rock mass is of prime importance for assessing the rock fall hazard. The "Roche du Midi" site, which was considered as a potential unstable rock due to the very open fracture F_1, was investigated using three types of techniques: direct field measurements, remote geodetic methods (terrestrial laser scan and photogrammetry) and geophysical techniques including GPR scans on the cliff face. The first two types of techniques only provide information at the surface while geophysical techniques allow the extent of the fractures at depth to be determined.

Four sets of fracturing data were measured on the site. Two of them correspond to direct sampling in the field: one on the plateau, around the unstable cliff (set Direct Measurement 1 or DM1), and the other one on the frontal face of the cliff itself when abseiling (set DM2). Two other sets come from the two remote techniques applied to the cliff: the solid image which combines a single photo and DDSM (data set Remote Technique 1 or RT1) and the parallel photogrammetry principle to restore the 3D geometry (data set RT2). The rose diagrams for these four data sets are shown in figure 10b. These four approaches give similar results in the way that they reveal a part of or the totality of the same fracture system. This system is made of two main families F_a striking N20°E ±10° and F_b striking N130°E ± 10°. The dip of both families is nearly vertical, 90° ±15°. If we consider data collected with technique DM1 representative of the massif fracturing, remote technique RT2 appears as a valuable alternative giving very similar results. In addition RT2 has the advantage to be performed on the potential unstable part of the cliff itself. Compared to DM2, RT2 is largely quicker, more accurate and safer. On the other hand, the second remote technique RT1, based on the solid image, suffers some sampling problems. Even if the same part of the cliff was observed with RT1 and RT2, the F_b family

was poorly detected by RT1. This default is due to the laser scanning illumination which was almost parallel to the fracture surfaces of family F_b for both views. It results in a very low density of the point cloud at these places, which did not permit the orientation of the F_b fractures. On the other hand, laser scanning data were used during the processing of the GPR traces. The position of the GPR profiles was computed from the DDSM (figure 5).

The continuity of the two fracture sets inside the massif is confirmed by the couples of horizontal and vertical GPR images (P1/P1h and P2/P2h). Figure 10a shows the 3D view for the profiles P1/P1h, along with the diagram of the available fracture measurements along the two profiles (figure 10b). The orientation of the fractures detected by GPR agrees with the measurements made at the surface. This validates the use of GPR as a tool for investigating the internal fracture pattern, if horizontal profiles can be performed, along vertical profiles. The penetration of radar waves on the site was usually between 20 and 25 m with the 100 and 200 MHz antennae, with the exception of Profile P3 where the penetration decreases to 10 m due to a weathered zone. This penetration range limits the application of the technique to objects with a maximum volume of a few tens of thousands m^3 in such limestone rocks. The unexpected and major information provided by all GPR images is the presence of a major and continuous fracture (F_2) dipping inwards the mass, which was not observed during the geological investigation. This result, which was not detected either during the initial geological investigation or by the geophysical techniques applied on the plateau, highlights the interest of using the GPR technique on the cliff face. This major discontinuity is parallel to the Montaud fault outcropping 500 m from the site. The existence of this fracture was validated by observations in the cliff karstic network. With the determined fracture pattern, the site does not present a short-term stability problem. If the hidden fracture F_2 had been found with a reverse dip (outwards the mass), the hazard would have increased dramatically.

This study on a particular site has shown the necessity of combining remote and ground imaging methods for characterizing the fracture pattern of potential unstable cliff sites. Further development would consider the use of laser scanning acquisition from a helicopter in order to adequately illuminate the cliff as well as the design of new GPR instruments allowing easy measurements on high nearly vertical faces.

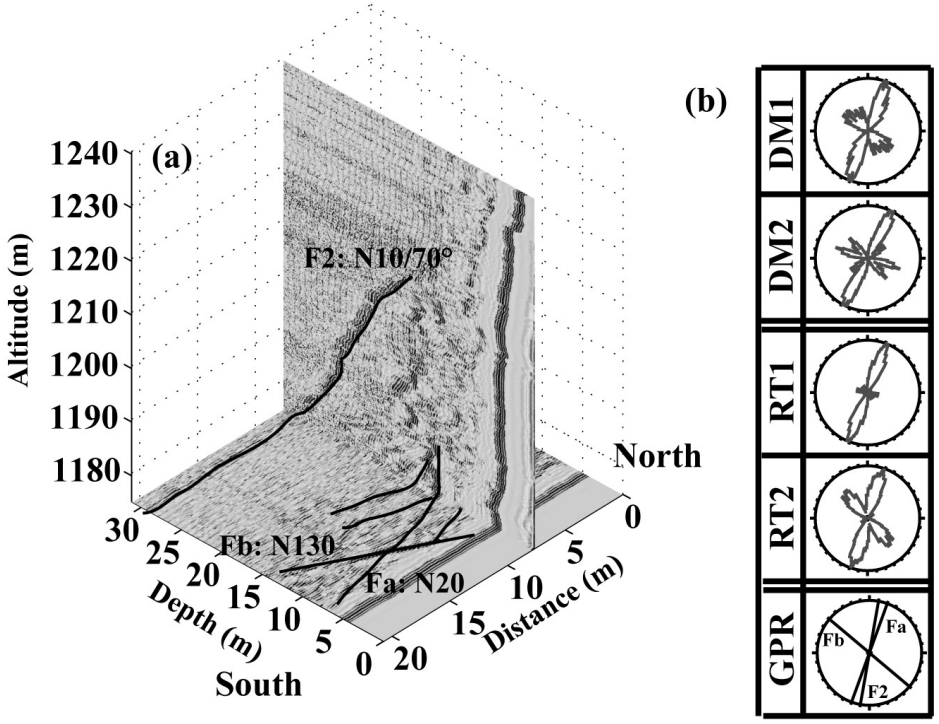

Figure 10: (a) 3D view of GPR images P1 and P1h with the fracture F_2 and the two discontinuity

families F_a and F_b. (b) Rose diagrams for the five data sets (DM1, DM2, RT1, RT2 and GPR).See text for detail.

Acknowledgements

This research was funded by the French national RDT program (CAMUS Project, Ministère de l'Ecologie et du Développement Durable). We thank Henry Mora for his help in adapting the GPR system to the cliff investigation. Leandro Bornaz and Paolo Maschio from DITAG at Politecnico Torino performed the laser scanning acquisition very professionally for us. We had helpful discussions with Prof Fulvio Rinaudo from the same institute about data treatment and geometrical bias. The solid image was computed with an academic version of LSR, software gently provided by DITAG. The solid image is now a trademark of SIR (www.sir.to.it). We thank all the numerous and enthusiastic participants to the field campaigns. The author used Seismic Unix for data processing and a RAMAC/GPR unit system (MAL? Geosciences) for acquisition. We thank Professor Scarascia-Mugnozza and two anonymous reviewers for their constructive comments.

References

Alberts, C.P. 2004 Surface reconstruction from scan paths. *Future Generation Computer Systems*, **20**, 1285-1298.

Ardizzone, F., Cardinali, M., Galli, M., Guzzetti, F. and Reichenbach, P. 2007 Identification and mapping of recent rainfall-induced landslides using elevation data collected by airborne Lidar. *Nat. Hazards Earth Syst. Sci.*, 7, 637–650,

Arnaud, H., Bravard, Y., Fournier, D., Gidon, M. and Monjuvent, G. 1978 *Carte géologique à 1/50000, feuille de Grenoble*. Tech. rept. BRGM Ed.

Arpin, R. 1988 *Déformations et déplacements des massifs subalpins de Vercors et Chartreuse*. Ph.D. thesis, Grenoble University, France.

Bornaz, L. and Dequal, S. 2003 The Solid Image: a new concept and its applications. *In: The International Archives of the Photogrammetry, Remote Sensing and Spatial Information Sciences*, vol. XXXIV, *Turchia*, 78-82.

Busby, J. and P., Jackson. 2006 The application of time-lapse azimuthal apparent resistivity measurements for the prediction of coastal cliff failure. *Journal of Applied Geophyiscs*, **59**, 261-272.

Chen, R.-F., Chang, K.-J., Angelier, J., Chan, Y.-C., Deffontaines, B., Lee, C.-T., Lin and M.-L. 2006 Topographical changes revealed by high-resolution airborne LiDAR data: The 1999 Tsaoling landslide induced by the Chi–Chi earthquake. *Engineering Geology* **88**, 160–172.

Deparis, J. and Garambois, S. 2006 Fracture Imaging and Characterization from APVO GPR Data. *In: 11th Int. Conf. on Ground Penetrating Radar, United State, 6p*.

Deparis, J., Garambois, S. and Hantz, D. 2007 On the potential of Ground Penetrating Radar to help rock fall hazard assessment of a limestone scale, *Engineering Geology*, **94**, 89-102, 2007

Dussauge-Peisser, C., Wathelet, M., Jongmans, D., Hantz, D., Couturier, B. and Sintes, M. 2003 Seismic tomography and ground penetrating radar applied on fracture characterisation in a limestone cliff, Chartreuse massif, France. *Near surface geophysics*, **1**, 161-172.

Feng, Q.H. and Röshoff, K. 2004 In-situ mapping and documentation of rock faces using full-coverage 3d laser scanning technique. *In: ISRM SINOROCK 2004 Symposium, China*, 139-144

Glenn, N.F., Streutker, D.R., Chadwick, D.J., Thackray, G.D., Dorsch, S.J. 2006 Analysis of LiDAR-derived topographic information for characterizing and differentiating landslide morphology and activity. *Geomorphology* **73**, 131–148

Gidon, M., Arnaud, H. and Monjuvent, G. 1978 *Notice de la carte géologique au 1/50000, feuille Grenoble*. BRGM Ed.

Hantz, D., Vengeon, J. M. and Dussauge-Peisser, C. 2003 An historical, geomechanical and probabilistic approach to rock-fall hazard assessment. *Natural Hazards and Earth System Sciences*, **3**, 693-701.

Heincke, B., Maurer, H., Green, A.G., Willenberg, H., Spillmann, T. and Burlini, L. 2006 Characterizing an unstable mountain slope using shallow 2 and 3-D seismic tomography. *Geophysics*, **71**, B241- B256.

Hoek, E. and Bray, J. 1981 *Rock slope engineering (revised third edition)*. London: Institution of Mining and Metallurgy London.

Jeannin, M., Garambois, S., Jongmans, D. and Grégoire, C. 2006 Multiconfiguration GPR measurements for geometric fracture characterization in limestone cliffs (Alps). *Geophysics*, **71**, B85-B92.

Jongmans, D. and Garambois, S. 2007 Geophysical investigation of landslides : a review. *Bull. Soc. géol. France*, **178**, 101-112.

McKean, J. and Roering, J. 2004 Objective landslide detection and surface morphology mapping using high-resolution airborne laser altimetry. *Geomorphology*, **57**, 331-351

Lemy, F. and Hadjigeorgiou, J. 2004 A field application of laser scanning technology to quantify. *In: EUROCK 2004 & 53rd Geomechanics, Austria,* 435-438.

Loke, M.H. 2000 *Electrical imaging surveys for environmental and engineering studies – a practical guide to 2D and 3D surveys*. short training course lecture notes, Geotomo Software, Peynang, Malaysia.

Loke, M.H. and Barker, R.D. 1996 Rapid least-squares inversion of apparent resistivity pseudosections by a quasi-Newton method. *Geophysical Prospecting*, **44**, 131-152.

Mikhail, E.M., Bethel, J.S. and McGlone, J.C. 2001 *Introduction to Modern Photogrammetry.* Wiley.

Peterson, J.E., J.T., Sullivan and Tater, G.A. 1982 The use of computer enhanced satellite imagery for geologic reconnaissance of dam sites. *In: ICOLD, 14th Cong. On Large Dams, Brazil, 449-471*.

Philippe, Y., Deville, E. and Mascle, A. 1998 *Thin-skin inversion tectonics at oblique basin magin : example of the western Vercors and Chartreuse Subalpine massifs.* Mascle A., Puigdefµabregas C., Luterbacher H., Fernµandez M. (eds) Geological Society, London, Special Publications. Pages 239-262.

Reynolds, J.M. 1997 *An introduction to applied and environmental geophysics.* John Wiley & Sons, Chichester, England.

Roch, KH., Chwatal, E. and Bräuckl, E. 2006 Potential of monitoring rock falll hazards by GPR : considering as example of the results of Salzburg. *Landslide*, **3**, 87-94.

Sahbi, H., Jongmans, D. and Charlier, R. 1997 Theoretical study of slope effects in resistivity surveys and applications. *Geophysical prospecting*, **45**, 795-808.

Schulz, T and Ingensand, H. 2004 Terrestrial Laser Scanning – Investigations and Applications for High Precision Scanning. *In: FIG Working Week, Greece, 15p*.

Schulz, T., Lemy, F. and Yong, S. 2005 Laser Scanning Technology for Rock Engineering Applications. *In: Optical 3-D Measurement Techniques VII (Eds. :Gräun, Kahmen), Austria*, 50-59.

Schulz, W.H 2007 Landslide susceptibility revealed by LIDAR imagery and historical records, Seattle, Washington. *Engineering Geology*, **89**, 67-87

Thoma, D.P., Guptab, S.C., Bauerc, M.E. and Kirchoff, C.E. 2005 Airborne laser scanning for riverbank erosion assessment. *Remote and Sensing Environment*, **95**, 493-501.

Tsakiri, M, Lichti, D and Pfeifer, N. 2006 Terrestrial laser scanning for deformation monitoring. *In: 3rd IAG / 12th FIG Symposium, Germany*, 10p.

van Asselen, S. and Seijmonsbergen, A.C. 2006 Expert-driven semi-automated geomorphological mapping for a mountainous area using a laser DTM. *Geomorphology*, **78**, 309-320.

Widess, M.B. 1973 How thin a thin bed ? *Geophysics*, **38**, 1176-1180.